



City Research Online

City, University of London Institutional Repository

Citation: Ravikumar, B., Karathanassis, I. K., Smith, T. & Gavaises, M. (2023). Dilute viscoelastic polymer solutions for dielectric heat transfer applications: A molecular dynamics study. *International Journal of Thermofluids*, 18, 100333. doi: 10.1016/j.ijft.2023.100333

This is the published version of the paper.

This version of the publication may differ from the final published version.

Permanent repository link: <https://openaccess.city.ac.uk/id/eprint/30136/>

Link to published version: <https://doi.org/10.1016/j.ijft.2023.100333>

Copyright: City Research Online aims to make research outputs of City, University of London available to a wider audience. Copyright and Moral Rights remain with the author(s) and/or copyright holders. URLs from City Research Online may be freely distributed and linked to.

Reuse: Copies of full items can be used for personal research or study, educational, or not-for-profit purposes without prior permission or charge. Provided that the authors, title and full bibliographic details are credited, a hyperlink and/or URL is given for the original metadata page and the content is not changed in any way.

City Research Online:

<http://openaccess.city.ac.uk/>

publications@city.ac.uk



Dilute viscoelastic polymer solutions for dielectric heat transfer applications: A molecular dynamics study

Bharath Ravikumar ^a, Ioannis K. Karathanassis ^{a,*}, Timothy Smith ^b, Manolis Gavaises ^a

^a School of Science and Technology, City, University of London, EC1V 0HB London, United Kingdom

^b Lubrizol European Research and Development Centre, Nether Lane, Hazelwood, DE56 4AN Derbyshire, United Kingdom

ARTICLE INFO

Keywords:

Viscoelastic liquids
Novel coolants
Thermal management
Molecular dynamics
Polymer solution

ABSTRACT

The suitability of industrially significant synthetic oils with dispersed polymeric chains that can be used as dielectric coolants with enhanced heat transfer properties in single-phase immersion cooling for electric vehicle components is evaluated via molecular dynamics simulations (MD). The fluids investigated are a synthetic solvent poly-alpha-olefin (PAO-2) and a solution based on PAO-2 with a single olefin co-polymer (OCP) chain dissolved. The simulation model accurately predicts the experimental thermodynamic properties of PAO-2. The effect of the polymer chain on the structural behaviour of the solution and its relation with the rheological properties is predicted and analysed at various temperatures in the range of 293 K–373 K. It is found that polymer solution shows an average viscosity enhancement of 9.2% and thermal conductivity enhancement of 2% within the temperature range. These properties eventually influence the Weissenberg and Nusselt numbers that impact the heat transfer. Analysis of the hydrodynamic radius of PAO-2 molecules shows that OCP chemistry acts as a thickening agent in the solution. Addition of the polymer chain is also shown to accelerate the shear thinning process due to increase in storage and loss moduli. The terminal relaxation time of OCP decreases with temperature and shear rate. The work conclusively establishes the impact of molecular interactions of the weakly viscoelastic liquids on their macroscopic behaviour. The viscoelastic nature of the examined polymer solution can lead to vortex roll-up in constricted flows inducing heat transfer enhancement. This in turn supports its use in immersion cooling applications which is shown for the first time.

1. Introduction

Effective thermal management of several electrical and electronic devices such as transformers, integrated circuits, electric motors and battery packs, among others constitutes a crucial aspect designating their performance [1,2]. Novel heat convection cooling concepts are actively pursued employing heat transfer liquids with properties tailored to the application of interest rather than relying on conventional coolants such as water or air [3–6]. Specifically referring to vehicle electrification technologies, the incorporation of suitable battery thermal management systems (BTMS) can allow faster battery charge/discharge rates, lead to smooth performance characteristics of the electric motor and high speed gear-box, and facilitate in increasing the battery life-time [7,8]. The current research on BTMS is scattered across single-phase forced convection [9] that does not provide the cooling efficiency required for heavy-duty vehicles, convective flow-boiling that requires large quantities of cooling liquid to be circulated, and pool-boiling immersed cooling technique [10] that cannot sustain beyond a few charge–discharge cycles. This is where single-phase

immersion cooling through dielectric liquids can be proposed as an attractive technique to cool electric vehicle components, especially the battery pack [11], and in addition, prevent huge pumping losses and eliminate the requirement of huge heat exchangers.

Along the lines of developing novel dielectric coolant fluids, identification of rheological properties capable of enhancing the underlying heat transfer processes is expected to maximise the effectiveness of future BTMS. New-generation coolants based on oils with macromolecule additives such as polymers and nanoparticles are investigated in recent literature [12–14]. These liquids show enhanced thermal properties, but at the same time have complex rheology exhibiting characteristics of both liquids and solids as a response to forces and time, leading to simultaneous flow, deformation and elasticity [15–17]. Dilute polymer solutions based on mineral, synthetic or silicone oils belonging to the category of complex-rheology fluids are seen as promising yet unexplored candidates to serve as heat transfer liquids. Unlike nanoparticles, the polymer chains at dilute concentrations do not significantly influence the bulk thermodynamic and transport properties of the oil,

* Corresponding author.

E-mail address: ioannis.karathanassis@city.ac.uk (I.K. Karathanassis).

nevertheless they modify its rheological behaviour in a manner that can be controlled using the polymer chemistry. The addition of long-chain polymers as viscosity modifiers (VM) in the base oil leads to the onset of flexible micelles that can form complex networks under shear [18]. This behaviour is macroscopically perceived as viscoelasticity, which can be tailored at the molecular scales to manipulate the fluid rheology in a pre-specified manner. Consequently, it helps in controlling the magnitude of vortices generated, which in turn leads to high heat transfer coefficients as explained recently by Wu et al. [19] Karathanassis et al. [20] linked the effects of the different chemistries of the polymers in dilute solutions and the vorticity-magnitudes in flows through complex hydraulic circuits. Khan et al. [21] showed that the dispersed polymers imparting viscoelasticity can stabilise vortices, and reduce the thermal boundary layer to increase the heat transfer. Thus, a viscoelastic liquid leading to increased vorticity in wall-confined flows, while also retaining the pressure-loss penalty moderate by its shear thinning nature, would constitute an ideal heat transfer medium for immersion cooling applications.

Viscoelastic fluids can also exhibit a shear thinning nature caused by stretching, alignment and decomposition of the microstructures [22, 23]. Pimenta and Campos [24] discussed how a combination of shear thinning and viscoelasticity in case of dilute polymer solutions lead to non-Newtonian behaviour that helps in the reduction of frictional losses, improving pumping performance. At the same time, it is shown that high elasticity hinders this reduction. In essence, a simultaneous understanding of their rheological and heat transfer characteristics is needed, since dimensionless numbers such as Weissenberg number (defined by viscosity and relaxation time) and Nusselt number (defined by thermal conductivity) eventually designate fluid cooling performance [25,26]. Parvar et al. [27] have recently reported how increasing elasticity of polymer solutions increase their Nusselt numbers and decrease the thermal boundary layer during laminar flow of these solutions.

To propose a liquid for an application where rheology and transport properties are of significance, we need to systematically characterise the relevant properties as a function of important operational parameters such as temperature. There are experimental challenges when it comes to analysing the properties related to the liquids of interest such as polymer relaxation time, normal stress differences, mixture viscosity as a function of shear, etc [28–31]. To give insights into the non-Newtonian characteristics bestowed upon by the addition of polymers, the properties of the polymer solution have to be compared to that of the base solvent. In this study, we simulate a widely available synthetic oil called poly-alpha-olefin (PAO-2) having a kinematic viscosity of 2 cSt or 2 mm² s⁻¹ at 373 K. The oil forms the base solvent of several lubricants. The PAOs have high viscosity index, high fluidity at lower temperatures and high oxidative/chemical stability. Such properties are beneficial for heat transfer applications [32]. In addition, lower molecular weight olefins such as PAO-2 exhibit biodegradable properties [33]. PAO-2 has a pour point of ~ 200 K [34], and is liquid at room temperature. The flash point is ~ 431 K [34] making it safer to use as a coolant in various electromechanical devices.

Among the polymer additives mixed in PAO-2 solvent used for industrial purposes, an ethylene-propylene co-polymer known as olefin co-polymer (OCP) is an important one [35]. The straight structural architecture and narrow molecular weight distribution of OCP make it a good thickener compared to other polymer chemistries [36]. OCP tends to behave differently based on the solvent it is dispersed in [37, 38]. Therefore, the thermophysical properties of a single OCP chain dissolved in PAO-2 solvent must be determined in order to study the extent of its capabilities. It eliminates any impact due to the polymer concentration and resulting entanglements, revealing its intrinsic nature.

Classical molecular dynamics (MD) constitutes an ideal modelling approach to conduct an in-depth property analysis of molecularly-specific polymer solutions. There are limited number of studies available in the open literature that focus on the computation of thermophysical properties of the fluid of our interest using atomistic MD [39,40].

In this study, we focus on how the molecular interactions impact the flow rheology. More specifically, we compare and contrast the properties of bare PAO-2 solvent and a single OCP polymer dispersed PAO-2 solution for temperatures in the range of 293 K and 373 K. The temperature range is significant to the operating conditions of electric vehicle components such as the Li-ion battery pack, electric motor and high speed gear-box [41–43]. We study the impact of the polymer chain on the molecular structural changes in the solution and see its relationship with the rheological properties. In addition to this, the thermal conductivity changes made by the polymer addition are also analysed in this investigation. The polymer solution shows improvement in shear thinning, and OCP shows flexible chain characteristics depicted by its radius of gyration in the solution. This work is the first to indicate the molecular basis for using oil-based solutions with dispersed polymeric chains for immersion-cooling applications.

2. Simulation details

Pure PAO-2 solvent, and the polymer solution consisting of a single OCP polymer chain in PAO-2 solvent at various temperatures and atmospheric pressure are simulated in this work. L-OPLS-AA [44,45] force-field of the following generic form is used in this simulation to model the interactions:

$$\begin{aligned}
 V(r) = & \sum_{bonds} k_b(b - b_0)^2 \\
 & + \sum_{angles} k_\theta(\theta - \theta_0)^2 \\
 & + \sum_{dihedrals} \sum_{n=1}^4 k_\phi(1 + (-1)^{n-1} \cos(n\phi)) \\
 & + \sum_{vdW} 4\epsilon_{ij} \left[\left(\frac{\sigma_{ij}}{r_{ij}} \right)^{12} - \left(\frac{\sigma_{ij}}{r_{ij}} \right)^6 \right] \\
 & + \sum_{Coulomb} \frac{q_i q_j}{\epsilon_0 r_{ij}}.
 \end{aligned} \tag{1}$$

Here, the first three terms on the right-hand side compute the bonded interaction energies due to bond stretching, bending and torsions. The last two terms compute the interactions due to van der Waals and electrostatic forces. The force-field parameters such as the bonding energies, Lennard-Jones (LJ) interaction parameters to model van der Waals energies, and partial charges to model the electrostatics are tabulated in Table S1 to Table S4 in the Supporting Information [44–48]. The LJ parameters (ϵ_{ij} and σ_{ij}) for the interactions between dissimilar atoms are computed as the geometric mean of the LJ parameters of the individual atom types (ϵ_{ii} and σ_{ii}).

In this study, 9,10-dimethyloctadecane (C₂₀H₄₂) is used to represent PAO-2 solvent, as the compound has been predominantly found in the PAO-2 oil [49]. The pure solvent simulation box is created using 170 molecules of 9,10-dimethyloctadecane [50]. The OCP polymer chain studied here is made up of 50 mole percent of ethylene (C2) monomers and 50 mole percent propylene (C3) monomers with a molecular mass of 3016 g mol⁻¹. The polymer of this particular weight and chain size is chosen as it provides low relaxation times representative of weakly viscoelastic liquids. The chain consists of 43 molecules each of C2 and C3 monomers with the two ends of the chain terminated using hydrogen atoms. Fig. 1 shows the schematic of the solvent and polymer chain molecular structure studied in this work. The polymer chain is added to the solvent simulation box to create a polymer solution of concentration ≈ 5.9 percent by weight. The individual molecules and the simulation box have been generated using Moltemplate software [51]. Hereafter, the pure PAO-2 solvent simulation system is termed as ‘pure solvent’ and the polymer solution system is termed as ‘polymer solution’, unless specified otherwise. The initial three-dimensional simulation box size of pure solvent is 100 × 100 × 100 Å³. The corresponding box size of polymer solution is 250 × 100 × 100 Å³. We apply periodicity in all 3 directions of the boxes to simulate bulk liquids.

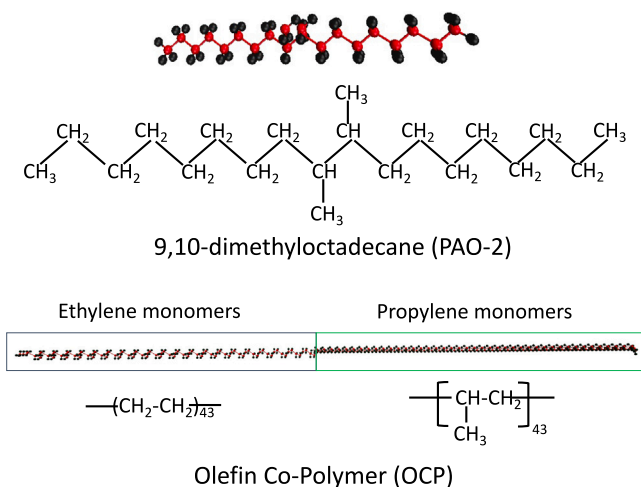


Fig. 1. Schematics of the solvent - PAO-2 molecule and polymer chain - OCP molecule used in this simulation study.

Large-scale Atomic/Molecular Massively Parallel Simulator (LAMMPS) [52] is used for the MD simulation of pure solvent and polymer solution. The study here is carried out to compute properties between a temperature range of 293 K and 373 K. The properties of the systems are computed at five different temperatures at intervals of 20 K for this purpose. We use Nosé–Hoover thermostat to maintain the temperatures at various stages of the equilibrium MD. The corresponding barostat as implemented by LAMMPS is used to set the pressures. The distance cut-off for van der Waals interactions is set to 13 Å. A faster Ewald summation methodology called particle–particle–particle-mesh (PPPM) is used to compute the long-range electrostatic interactions [53]. Velocity-verlet algorithm [54] is used to integrate the equations of motion with a time-step of 1 fs.

In order to model the alkanes having more than 16 carbon molecules by OPLS-AA force field, it is recommended to switch-off the 1–4 intra-molecular non-bonded pairwise interactions [39,55]. That is, the weighting coefficients of the computed pairwise forces and energies between the first and fourth atom connected covalently in a molecule is 0.0. However, in our case (while using L-OPLS-AA parameters) such a modification overestimates density values of pure solvent for temperatures between 313 K and 373 K by 0.01 g cm⁻³. To rectify it, we increase the weighting contribution of 1–4 intra-molecular non-bonded pairwise interactions for pure solvent systems to 0.5 for simulations between 313 K to 373 K. On the other hand, it is set to 0.0 at all temperatures for polymer solution to obtain appropriate thermodynamic properties.

Pure solvent and polymer solution systems remain liquids in the temperature range simulated. The equilibrium MD simulation protocol for a run at temperature, $T = 293$ K and pressure, $p = 1$ atm is as follows: The systems are initially energy-minimised using conjugate-gradient algorithm with tolerance values of 10^{-4} and 10^{-6} for energy and force calculations, respectively. Here, a larger neighbour-list skin cut-off of 6 Å is used to prevent the system from destabilisation. The energy-minimised systems further undergo a constant enthalpy (NPH) simulation for 2000 fs using a Langevin thermostat at the desired temperature. This step is used to expedite the process of equilibration [50,56]. Following that, the system is further equilibrated under NPT conditions where Nosé–Hoover thermostat and corresponding barostat are applied to maintain temperature and pressure, respectively. The changes in stress occur isotropically. At this stage, the neighbour-list cut-off is reduced to 2 Å to speed-up computations. Once the system is equilibrated for 20 ns under NPT, the resulting configuration undergoes an annealing process where, the simulation system is gradually run at higher temperatures of 298 K, 303 K, 308 K, 313 K and 318 K for

Table 1

Comparison of density (ρ_0) of pure solvent systems with experimental values (see Supporting Information for further details), and simulated values [50] from literature.

Temperature (K)	Present simulation (g cm ⁻³)	Experimental/Literature (g cm ⁻³)
293	0.800 ± 0.005	0.793 (Table S5)
313	0.780 ± 0.005	0.780 ± 0.005 [50]
333	0.764 ± 0.005	0.766 (Table S5)
353	0.748 ± 0.005	0.752 (Table S5)
373	0.732 ± 0.006	0.733 ± 0.005 [50]

1 ns each under constant NVT conditions. The system is rapidly brought back to 293 K following that under NVT and run for 1 ns to complete the process of annealing. The time invariance of the radial distribution functions of atoms as shown in Figure S1 in the Supporting Information establishes that the system is well equilibrated after these steps. The equilibrated and annealed system is used for a production run of 40 ns under NVT. The trajectories of the atoms are stored at regular intervals to compute the properties. The reported values of properties at a typical temperature are obtained from three independent runs. The protocol followed to compute properties using non-equilibrium MD methods is discussed in the relevant sections below.

3. Results and discussion

The following section discusses the different computational approaches used to determine the various properties, and assesses the results. The force-field is validated initially for the pure solvent system comparing the density (ρ) values against data available in the literature. The simulated isothermal compressibility (κ_T) of pure solvent is also compared against experimental measurements to validate the thermodynamics of the system. The transport properties such as self-diffusion coefficient, zero-shear viscosity, and thermal conductivity are computed and compared in case of pure solvent and polymer solution systems. Furthermore, the shear thinning behaviour of the liquids and the underlying reasons owing to their molecular interactions are analysed. Subsequently, the relaxation times of the polymer as a function of temperature and shear rate are estimated to characterise the viscoelastic nature of the polymer solution.

3.1. Thermodynamic properties of pure solvent

The validation of the force-field is done by computing certain important properties and verifying its agreement with data in the available literature. In this work, PAO-2 is treated as a homogeneous compound of 9,10-dimethyloctadecane. Therefore, it is important to see how well the thermodynamic properties represent the actual PAO-2 oil.

The first property analysed is the pure solvent density (ρ_0). The densities are computed from the NPT equilibration runs for pure solvent. The average values are reported in Table 1 along with their standard deviations. As expected, ρ_0 of pure solvent decreases with temperature. Comparison of the values with the data in the available literature shows a good agreement.

In addition to density, isothermal compressibility (κ_T) is an important feature that needs to be computed as compressibility of liquids is related to rheology in certain extreme conditions [57]. Isothermal compressibility of pure solvent in our case is found using the following simulation protocol: The atomic configurations after NPT simulation at $p = 1$ atm are subjected to a set of simulations with p varied from 10 to 1000 atm at a given temperature. The NPT simulation at every p lasts for 10 ns. Density is computed from the average of the final 5 ns run at all conditions of pressure. The data thus obtained is fitted to the modified form of Tait equation [58],

$$\rho = \frac{\rho_0}{1 - C \log_{10} \left(\frac{p+B}{\rho_0+B} \right)} \quad (2)$$

Table 2

Tait Equation parameters (B and C) and Isothermal compressibility (κ_T) of pure solvent systems at various temperatures, and comparison with experimental values. The experimental methodology is described in the Supporting Information.

Temperature (K)	B (MPa)	C	Simulated $\kappa_T \times 10^{11}$ (Pa $^{-1}$)	Experimental $\kappa_T \times 10^{11}$ (Pa $^{-1}$)
293	83.58	0.1538	79.42	79.55
313	114.01	0.2168	82.53	89.98
333	101.74	0.213	90.85	101.7
353	74.55	0.191	111.1	115.22
373	43.81	0.149	147.4	–

Here, ρ_0 is the density of pure solvent at $p_0 = 1$ atm (101325 Pa). The fitting constants C and B are related to κ_T as

$$\kappa_T = \frac{C}{2.302(p_0 + B)}. \quad (3)$$

B and C values, and comparison of κ_T with the experimental data are shown in Table 2. The ρ data as a function of pressure and the modified Tait equation fits are present in the Supporting Information (see Figure S2). Simulated κ_T values show a good match with the experimental data. The deviations observed can be attributed to the difference in the empirical model used for the computation of κ_T experimentally (see Equation S4 in the Supporting Information).

The computed thermodynamic properties show that use of L-OPLS-AA force-field and 9,10-dimethyloctadecane as a surrogate for PAO-2 oil are suitable to represent the systems of our interest in MD simulations. Therefore, we model polymer solution using the same force-field. Please see Table S6 in the Supporting Information for the thermodynamic properties of the simulated polymer solution. The other computed properties and their physical significance are described in the following sections.

3.2. Zero-shear viscosity

The Newtonian dynamic viscosity (η_0) is the most fundamental transport property measured to analyse the flow behaviour of the complex heat transfer liquids [59,60]. The variation in η_0 is an indication of the translational resistance to flow [61]. It is computed in MD using the Green-Kubo method based on the fluctuation-dissipation theorem of systems in equilibrium. η_0 is computed by the integration of a decaying stress auto-correlation function [62], such that

$$\eta_0 = \frac{V}{k_{BT}} \int_0^\infty \langle \sigma_{xy}(t) \sigma_{xy}(0) \rangle dt. \quad (4)$$

Here, V is the volume of the simulation box, k_B is the Boltzmann constant and $\sigma_{xy}(t)$ is one of the off-diagonal component of the stress tensor at time t . The statistics of η_0 computation is improved by taking an average of the auto-correlation function of the three off-diagonal components of the stress-tensor. In case of oils, the values of viscosity are reported in terms of kinematic viscosity (ν_0) given as

$$\nu_0 = \frac{\eta_0}{\rho}. \quad (5)$$

Fig. 2 shows ν_0 at various temperatures for pure solvent. Our simulated values are close to the reported experimental and simulation results of PAO-2 in literature [50,63]. The viscosity values decrease with temperature, which is expected in case liquids of this nature [64, 65]. As also shown in Fig. 2, the simulated values of polymer solution are higher than those of pure solvent at all temperatures. This implies that OCP polymer leads to viscosity enhancement when added to the PAO-2 solvent.

The relationship of viscosity of polymer solutions with temperature can be modelled using an Arrhenius-like equation

$$\ln(\nu_0) = \ln(\nu_{0c}) - \frac{E_a}{RT} \quad (6)$$

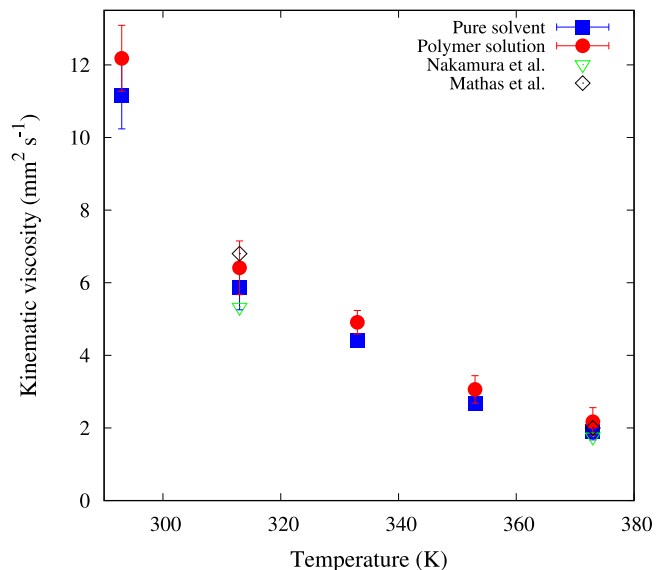


Fig. 2. The kinematic viscosity (ν_0) of the pure solvent system and polymer solution as a function of temperature. The closed symbols represent the average of simulated values—red (Pure solvent) and blue (Polymer solution) with their standard deviations from the three independent runs. The open symbols represent the experimental [63] (green) and simulated [50] (black) data available in the literature for pure solvent system.

fitted to the data of ν_0 vs. $1/T$. Here, ν_{0c} and E_a are the fit constants. The E_a values are dependent on the nature of polymer and solvent, and polymer concentration [66,67]. Figure S3 in the Supporting Information shows the Arrhenius fits to the data for pure solvent and polymer solution systems. The E_a values of the former is 21.0 ± 1.6 kJ mol $^{-1}$ and of the latter is 20.3 ± 1.7 kJ mol $^{-1}$. The values show that at this concentration of OCP, the polymer does not cause a significant impact on the temperature dependence of the viscosity of the solution.

Given that the viscosity rise with addition of OCP polymer chain, we can look if the molecular transport of the different components due to thermal motion supports the observation. We compute self-diffusion coefficient in this regard.

3.3. Self-diffusion coefficient

The self-diffusion coefficient (D) is a measure of the translational movement of atoms and molecules due to the thermal energy of the system. In case of long-chain hydrocarbon systems, D can be computed for the constituent atoms, monomers (in case of polymers) or the centre of mass (COM) of the molecules. In our case we compute D of COM (D_{COM}). Usually, D_{COM} of a homogeneous system is inversely related to η_0 . MD uses Einstein's relation [68,69] to compute D_{COM} such that

$$D_{COM} = \frac{1}{6} \lim_{t \rightarrow \infty} \frac{d}{dt} \langle [\mathbf{r}_{COM}(t) - \mathbf{r}_{COM}(0)]^2 \rangle \quad (7)$$

where $[\mathbf{r}_{COM}(t) - \mathbf{r}_{COM}(0)]^2$ is the mean squared displacement (MSD) of the centre of mass of a molecule. The symbol $\langle \rangle$ is the ensemble average symbol. The relationship is applicable at long-time limits, where the MSD enters the linear regime. Here, the slope of MSD (computed via multiple time origins) beyond 10^5 fs from a linear function fit is used to compute D_{COM} (see Figure S4 in the Supporting Information). Fig. 3(a) shows the variation of D_{COM} with temperature of molecules in case of pure solvent and polymer solution.

$D_{COM,PAO}$ is system-size independent as shown by the comparison of the MSD values of a larger pure solvent system consisting of 340 molecules with the one studied here (see Figure S5 in the Supporting Information). With increase in temperature, pure solvent shows an increase in $D_{COM,PAO}$. This behaviour is opposite to that of the Newtonian

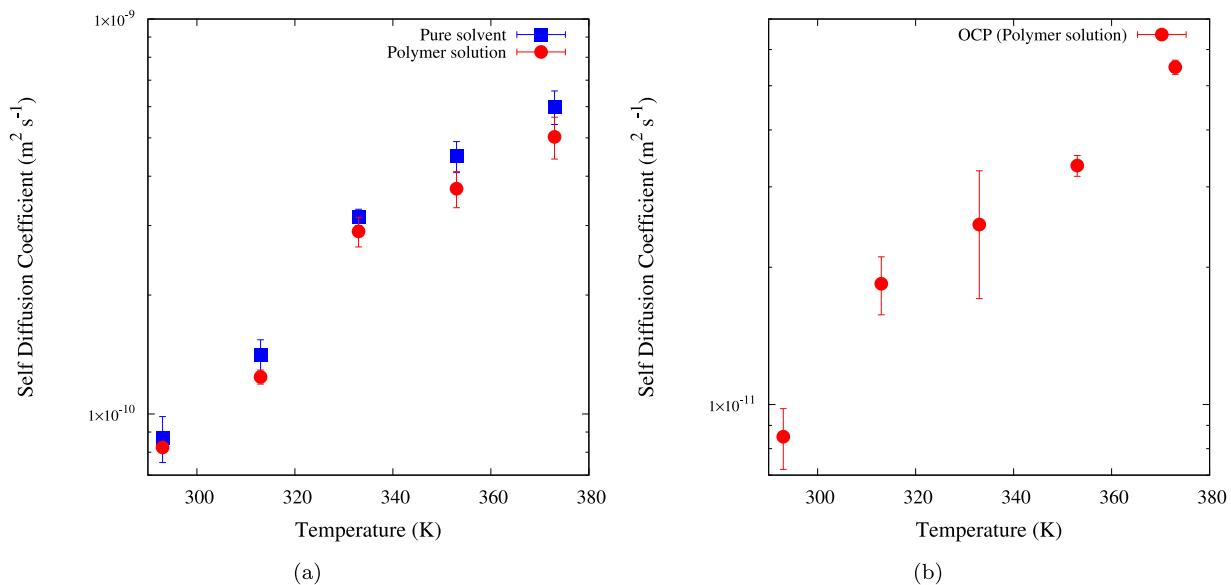


Fig. 3. The centre of mass self diffusion coefficient of (a) PAO-2 molecules ($D_{\text{COM,PAO}}$) in the pure solvent and polymer solution systems, and (b) OCP molecule ($D_{\text{COM,OCP}}$) in the polymer solution system as a function of temperature.

viscosity as a function of temperature. The implication is that kinetic energy gained by the molecules with increase in temperature assists in overcoming intermolecular forces of attraction (that causes resistance to motion). Coming to the polymer solution, we compute the diffusivity of PAO-2 solvent molecules and diffusivity of OCP polymer chain. The $D_{\text{COM,OCP}}$ of the polymer is considerably lower (by an order of magnitude) compared to that of the solvent molecules at all temperatures (see Fig. 3(b)). This is expected in case of a large molecule such as OCP. The addition of OCP decreases the D_{COM} of PAO-2 molecules as seen in Fig. 3(a) indicating that the polymer chain restricts the free motion of PAO-2 molecules. This relates to the enhancement in viscosity of the polymer solution system compared to that of the pure solvent system.

A direct impact of the polymer additive as a VM in polymer solution is observed from the analysis of the transport properties. Therefore, it is imperative to further look into the mechanism of viscosity enhancement in case of polymer solution. For that purpose, we have to probe the structural characteristics of the pure solvent and polymer solution systems as shown later in the article.

3.4. Couette flow

The primary objective of the rheological characterisation is to elucidate the non-Newtonian behaviour of the polymer solution. In order to do so, we first analyse the shear response of the pure solvent and polymer solution systems by simulating a Couette flow of the bulk liquids. We use a non-equilibrium MD (NEMD) simulation methodology to carry out the simulations, which enables the characterisation of shear thinning onset in the examined fluids.

The Couette flow of an MD simulation box with periodic conditions is implemented here by deforming the box in y -direction. A Lee-Edwards boundary condition is applied to ensure stability of the system [70,71]. We use SLLOD equations of motion to solve for the trajectories of the atoms as derived by Hoover and Ladd, and Evans and Morris [72,73]. They ensure the conservation of momentum, and account for the accurate values for dissipated energy. The extent of deformation can be defined in LAMMPS by a constant engineering shear strain rate ($\dot{\gamma}$). The resulting flux of stress (σ_{yz}) is used to compute the viscosity ($\eta(\dot{\gamma})$) as a function of the $\dot{\gamma}$ such that

$$\eta(\dot{\gamma}) = \frac{\sigma_{yz}}{\dot{\gamma}}. \quad (8)$$

In atomistic MD, the flow is established only at very high $\dot{\gamma}$, which is not experimentally achievable, and this constitutes as a shortcoming of MD [74]. However, we can still characterise the rheological behaviour by fitting the following Carreau-model to the data of $\eta(\dot{\gamma})$ vs $\dot{\gamma}$:

$$\eta(\dot{\gamma}) = \frac{\eta_0}{(1 + (\tau_s \dot{\gamma})^2)^m}. \quad (9)$$

Here, η_0 is the Newtonian viscosity that is obtained from the extrapolation of the data to $\dot{\gamma} = 0$. m is the strain-rate sensitivity coefficient. τ_s is the time constant referring to the shear rate where the shear thinning begins. $\dot{\gamma}$ values between the range of 10^8 s^{-1} and 10^{11} s^{-1} are applied to the simulation box. The model has been shown to fit the response of viscosity as a function of shear rate quite well in case of long chain hydrocarbons in the MD literature [40,55].

Fig. 4(a) shows the viscosity vs shear rate data and the corresponding Carreau-model fits at 313 K and 373 K. As seen, the simulated data has large error bars at lower shear rates and their magnitudes decrease at higher shear rates. It can be clearly discerned that η_0 of polymer solution is greater than that of pure solvent at both the temperatures. The comparison of η_0 computed by equilibrium MD from Eq. (4) and by NEMD from Eq. (9) in Table S7 in the Supporting Information shows fairly good agreement at all temperatures.

A polymer additive that increases the viscosity of a solvent can either be a thickening agent or a viscosity index improver (VII). OCP can be classified as the former if the increase in viscosity is independent of temperature, whereas it is classified as the latter if it increases viscosity only at higher temperatures. A method to identify if a polymer really acts as a VII or simply as a thickening agent is to compute the Q factor [55]. It is computed as

$$Q_{\text{VI}} = \frac{\eta_{sp,373\text{K}}}{\eta_{sp,313\text{K}}}, \quad (10)$$

where $\eta_{sp,373\text{K}}$ and $\eta_{sp,313\text{K}}$ are the specific viscosities at 373 K and 313 K, respectively, calculated as

$$\eta_{sp} = \frac{\eta_{\text{solution}} - \eta_{\text{solvent}}}{\eta_{\text{solvent}}}. \quad (11)$$

$Q_{\text{VI}} \leq 1$ for a substance that acts more as a thickening agent and $Q_{\text{VI}} \gg 1$ for an additive that acts more as a VII.

Table 3 shows the parameters of the Carreau-model for pure solvent and polymer solution systems. The fitted curves (as shown in Fig. 4(a)) have R-squared values greater than 0.95. The Q factor computed from the η_0 values is 0.86. This is indicative of the uniform thickening nature

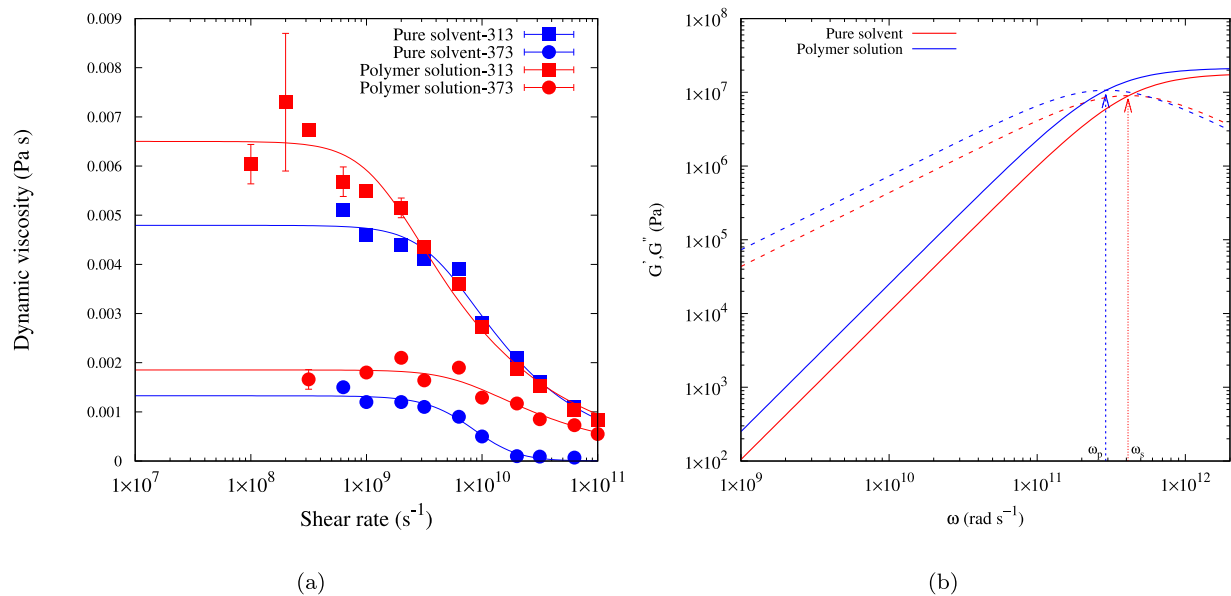


Fig. 4. (a) Viscosity ($\eta(\dot{\gamma})$) as a function of shear rate ($\dot{\gamma}$) at two different temperatures (313 K and 373 K) in pure solvent and polymer solution systems. The symbols with the error bars show the simulated dynamic viscosity values, $\eta(\dot{\gamma})$ at different shear rates, $\dot{\gamma}$. The lines depict the Carreau-model fittings. (b) The storage modulus, G' (solid) and the loss modulus, G'' (dashed) as functions of ω at a temperature of 313 K with the arrows indicating the cross-over ω values for pure solvent (ω_s) and polymer solution (ω_p).

Table 3
Parameters of Carreau-model (η_0 , τ_s , p) at various temperatures.

Pure solvent			
Temperature (K)	η_0 (Pa s)	τ_s (ns)	m
293	0.009	0.62	0.30
313	0.0048	0.31	0.28
333	0.0033	0.22	0.31
353	0.0021	0.20	0.24
373	0.0013	0.10	1.32
Polymer solution			
Temperature (K)	η_0 (Pa s)	τ_s (ns)	m
293	0.0130	0.95	0.26
313	0.0065	0.73	0.22
333	0.0039	0.34	0.23
353	0.0025	0.21	0.22
373	0.0017	0.14	0.22

of the OCP polymer chain when added to PAO-2 solvent. It confirms the observations derived from experimental investigation of OCP of higher molecular weights and different compositions [37]. The study here substantiates that it is the intrinsic nature of OCP chain to act as a thickening agent in an olefin-based oil, independent of the composition or dispersity of the polymer.

While comparing the τ_s values in Table 3 for pure solvent as a function of temperature, we see that they decrease with temperature. In case of polymer solution, τ_s decreases with temperature as well. However, the τ_s values are higher in case of the polymer solution compared to that of pure solvent. This indicates that addition of OCP enhances the shear thinning behaviour of the simulated polymer solution. The viscoelastic nature of the polymer chain contributing to this phenomenon can be verified by comparing the storage (G') and loss moduli (G'') of the two different liquids. In order to compute the two moduli, the integrand function in Eq. (4)

$$G(t) = \frac{V}{k_{BT}} \langle \sigma_{xy}(t) \sigma_{xy}(0) \rangle \quad (12)$$

is fit with an exponential function

$$G(t) = G_0 e^{-\left(\frac{t}{\tau_f}\right)} \quad (13)$$

with a single Maxwell mode, as implemented generally in case of macroscopic models of polymer chains such as finite extensible non-linear elastic polymer (FENE-P) model [75]. The τ_f value represents relaxation time of the fluid, and G_0 represents the ordinary elastic shear modulus. From the Fourier transformation of the above equation, the storage and loss moduli can be further obtained from the following relationships:

$$G'(\omega) = G_0 \frac{\omega^2 \tau_f^2}{1 + \omega^2 \tau_f^2} \text{ and } G''(\omega) = G_0 \frac{\omega \tau_f}{1 + \omega^2 \tau_f^2}. \quad (14)$$

The correlation data in Eq. (12) is smoothed by following the process recommended in literature before applying Eq. (13) to the data [76] (see Figure S6 in the Supporting Information). Fig. 4(b) shows G' and G'' as functions of ω at 313 K. As observed, the addition of polymer leads to an increase in the values of $G'(\omega)$ and $G''(\omega)$. This indicates that polymer solution has higher elasticity and viscosity, respectively than the pure solvent. The inverse of the ω where the crossing of $G'(\omega)$ and $G''(\omega)$ happens, provides the fluid relaxation time. As expected, ω of the polymer solution (ω_p) is lower than that of the pure solvent (ω_s). In other words, the relaxation time increases with the addition of the polymer chain in the solvent. This enhances the vortex roll-up and subsequent thermal behaviour of the polymer solution compared to that of the solvent.

It is natural for long-chain hydrocarbon solvents to showcase shear thinning at very high shear rates simulated in MD even though the shear rates at which macroscopic flow is observed, i.e., between the range of 10^1 – 10^6 s⁻¹, portray them as Newtonian. The reasons for the shear thinning nature of oil and long-chain hydrocarbons are described in the literature [77–79]. Given this scenario, the shear thinning of polymer solution triggered at lower shear rates than that for solvent emerges from the impact of polymer on the molecular interactions [80]. Therefore, the consistent enhancement of viscosity and the shear thinning behaviour at all temperatures observed with the addition of OCP requires further understanding in terms of the structural changes at the molecular level.

3.5. Structural characteristics

In the general polymer theory [81,82], the reason for increasing viscosity as a function of temperature of a polymeric fluid is attributed

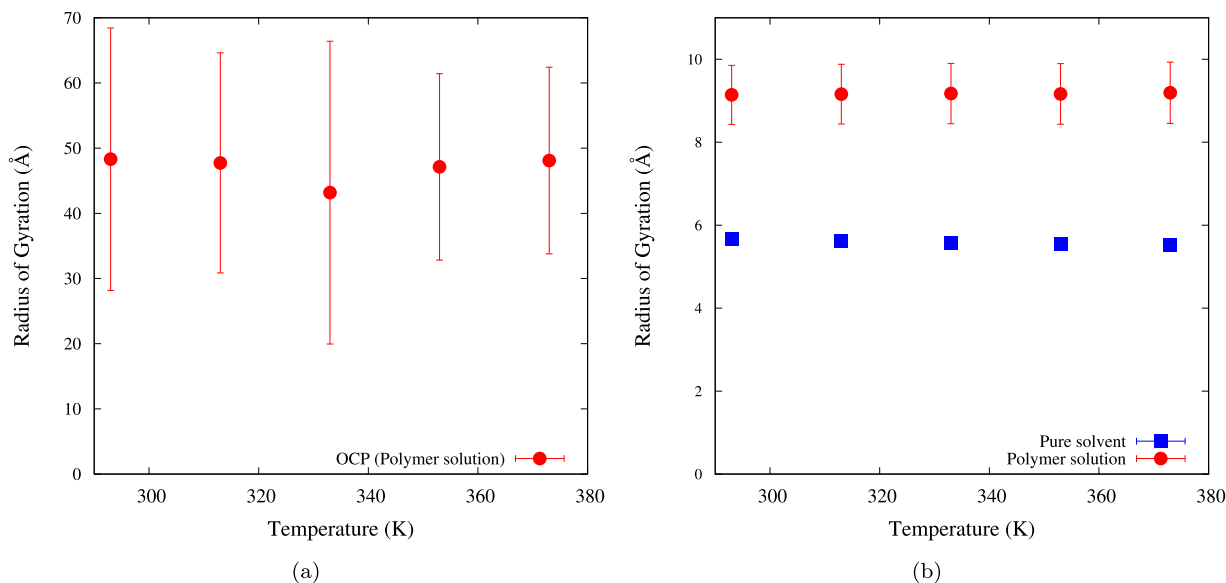


Fig. 5. The radius of gyration (R_g) of (a) OCP molecule in the polymer solution, and (b) PAO-2 molecules in the pure solvent and polymer solution as a function of temperature. The error bars show the standard deviation computed from the R_g values obtained at every 2 ps in the three independent runs.

to increasing hydrodynamic radius of the polymer chain. As temperature increases, the polymer chains expand which in turn improves the viscosity of the polymer fluids. A measure of the hydrodynamic radius is given by the radius of gyration (R_g) computed by the equation

$$R_g = \sqrt{\frac{1}{M} \sum_{i=1}^n m_i (\mathbf{r}_i - \mathbf{r}_{\text{com}})^2} \quad (15)$$

where M is the mass of a molecule, m_i is the mass and \mathbf{r}_i is the position vector of an atom i of a molecule consisting of n atoms. The computed values of R_g of the OCP polymer are shown in Fig. 5(a). The large error bars at every temperature depict the relative ease with which the shape of polymer chain changes. The mean values of R_g of OCP do not depict a significant monotonic increase as a function of temperature. This is in line with the findings in literature that exhibit that polymer chains composed of aliphatic monomers do not show an increase in R_g with temperature when dissolved in aliphatic solvents [37]. Therefore, polymer coil expansion cannot be considered as the reason for viscosity improvement with temperatures for all the chemistries.

Another important factor that can be probed as the reason for viscosity improvement is the impact of temperature on the solvent molecules configuration in polymer solution. Here, we compare and contrast the hydrodynamic radii of PAO-2 molecules in pure solvent and polymer solution systems. Fig. 5(b) shows the R_g of PAO-2 molecules in the two different liquids. The data clearly presents that there is a significant jump in the R_g of PAO-2 molecules in polymer solution from the R_g of the same in pure solvent. However, the mean values are constant as a function of temperature. It implies that the impact of thickening of the solvent due to the presence of OCP polymer is uniform throughout the temperature range. The relationship of this behaviour with dissolved OCP chemistry has been sparsely studied. Few reasons suggested in existing literature are lack of long side chains to improve the solubility in olefins at higher temperatures [83], and absence of oxygen atoms in OCP chain that can change its conformations significantly at different temperatures [39,84]. Even though not dealt in the present study, it is important to further probe on the causes for why OCP remains a weak VII in solvents such as PAO-2.

As discussed in the previous section, the shear thinning observed in case of these liquids with deformation can be attributed to their molecular configurations. The configurational changes contributing to this phenomenon is an interplay of chain stretching, tumbling, and molecular alignment [77,85–87]. Firstly, to analyse the impact of stretching, the computation of the end-to-end distances (R_e) of the solvent

molecules and the polymer chain is done. In our case, we use the position vectors of the carbon atoms at the terminal ends of the PAO-2 and OCP for the purpose of the computation of R_e of molecules. The end-to-end distance as a function of shear rate shows the significance of polymer stretching on the shear thinning behaviour (see Figure S7 in the Supporting Information). R_e of OCP increases from 22 Å at zero shear rate to 25 Å at the highest shear rate simulated, implying stretching. At the same time, R_e of PAO-2 molecules remains constant as a function of $\dot{\gamma}$ indicating that a maximum stretch has already been attained by the solvent molecules at zero shear rate.

A method to assess the alignment of the molecules as a response to the shear has been discussed by Datta et al. [88] in coarse-grained simulations. It involves the computation of the ratio of the y-component of squared end-to-end distance (R_{ey}^2) of the molecules to the total squared end-to-end distance such that

$$S_{\text{alignment}} = \frac{\langle R_{ey}^2 \rangle}{\langle R_e^2 \rangle}. \quad (16)$$

This ratio provides the fraction of molecular stretching aligned in the direction of the shear (y-direction). We apply the same methodology in this work. $S_{\text{alignment}}$ should be ideally 1/3 in the absence of any shear as the alignment of PAO-2 molecules should be independent of the direction.

Fig. 6 shows the variation of $S_{\text{alignment}}$ of solvent molecules as a function of $\dot{\gamma}$ at 313 K. The value of $S_{\text{alignment}}$ at $\dot{\gamma} = 0$ is shown on the y-axis and as expected, it is ≈ 0.33 . The value of $S_{\text{alignment}}$ increases with increasing shear rate, indicating the alignment of the molecules in the direction of the applied shear and reaching an upper plateau of ≈ 0.79 . This makes the liquids susceptible to shear thinning by lowering the fraction of molecules stretching in non-shear directions that create obstacles to shear flow. Consequently, they end with a lower Newtonian viscosity at very high shear rates. While assessing the $S_{\text{alignment}}$ of OCP polymer as a function of shear rate in Fig. 6, we observe a rise in the values to 0.49 in the shear rate range where shear thinning is seen and subsequent drop back to 0.35 once the viscosities reach lower Newtonian plateau. This shows the additional role of alignment of polymer chain stretching on the shear thinning of polymer solution. It is also important to analyse the tumbling effects of OCP chain on the shear thinning observed. However, this is out of the scope of the current study.

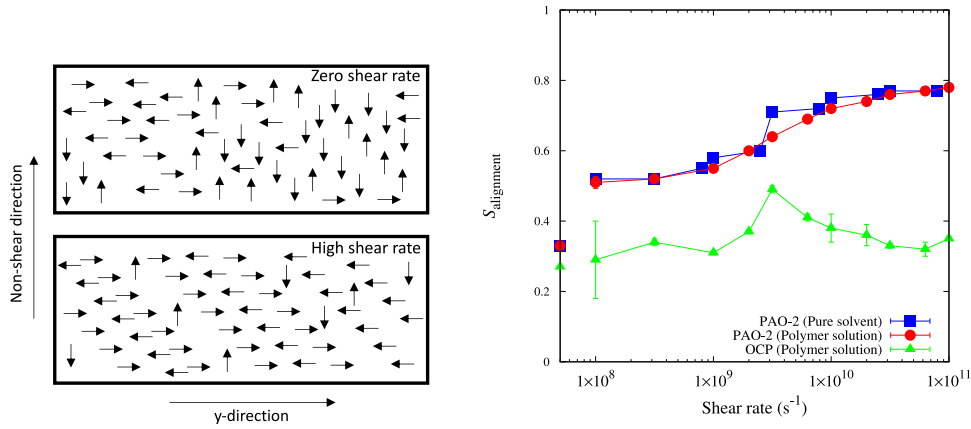


Fig. 6. (Left) The schematic of molecular alignment in the absence and presence of shear. (Right) $S_{\text{alignment}}$ of PAO-2 and OCP molecules in pure solvent and polymer solution as a function of shear rate at 313 K. The data points on the y-axis show the values of $S_{\text{alignment}}$ at zero shear rate.

We observed here how the addition of the OCP polymer chain influences the viscosity of the resultant polymer solution, and how molecular stretching and alignment influence the shear thinning behaviour of the liquids. We need to further characterise the viscoelastic effects of the polymer chain in the polymer solution systems by computing the polymer relaxation time.

3.6. Terminal relaxation time

Under specific circumstances, the viscoelastic behaviour has been linked to the vortex stabilisation and their lifetime [19,21]. The relaxation time provides a fundamental way to quantify the non-Newtonian viscoelastic behaviour of the liquids. It provides a measure of the time scale during which elastic stresses of polymer coil relax [89]. In case of a single chain of polymer, the longest relaxation time is attributed to the relaxation of the entire chain [90]. It is also called the terminal relaxation time (τ_R) of the polymer chain. Here, τ_R is computed as a function of temperature (using equilibrium MD), and shear rate (using NEMD).

The polymer chain showed that R_g does not vary significantly as a function of temperature. Therefore, it is important to see the extent of the polymer chain relaxation at different temperatures. For this, we use the end-to-end vector autocorrelation given as

$$C(t) = \frac{\langle \mathbf{R}(t) \cdot \mathbf{R}(0) \rangle}{\langle \mathbf{R}(0) \cdot \mathbf{R}(0) \rangle} \quad (17)$$

where, $\mathbf{R}(t)$ is the end-to-end vector ($\mathbf{r}_1 - \mathbf{r}_l$) of the OCP polymer chain having l monomers. The position vectors of the carbon atoms at the terminal ends of the chain are stored every 10 ps during the simulation run for the purpose of computation. We fit the $C(t)$ using a sum of three exponential functions as in

$$C(t) = \sum_{i=1}^3 \alpha_i e^{-\frac{t}{\beta_i}} \quad (18)$$

such that the integration of the function gives the terminal relaxation time

$$\tau_R = \int_0^{\infty} C(t) dt. \quad (19)$$

A sample of the $C(t)$ and the fit as described by Eq. (18) is shown in Figure S8 in the Supporting Information.

The τ_R values of OCP polymer as a function of temperature is shown in Fig. 7. The obtained values are in the order of nanoseconds. Even though relaxation times of this order of magnitude are plausible for such dilute polymers, it is not possible to compute them using the existing experimental apparatuses [91,92]. The values clearly show that the terminal relaxation time of the polymer chain decreases with temperature.

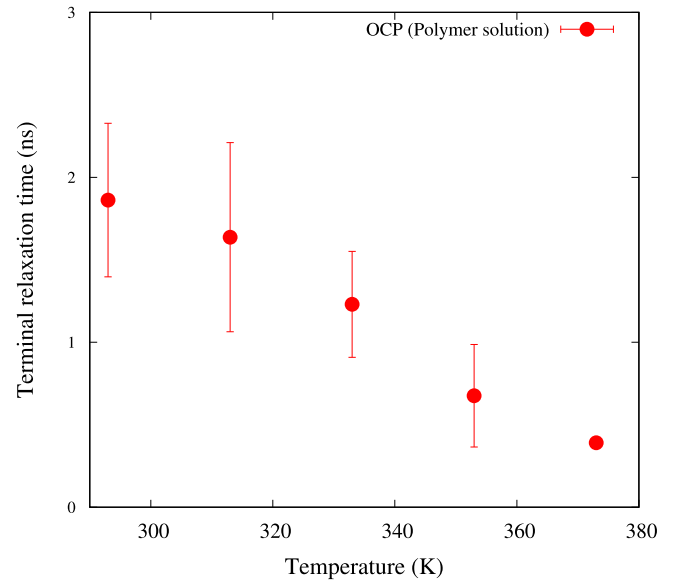


Fig. 7. The terminal relaxation time (τ_R) of OCP in the polymer solution as a function of temperature.

Understanding the response of the polymer chain relaxation as a function of shear rate is also vital to prescribe the complex fluid. Here, we compute τ_R as a function of $\dot{\gamma}$ by implementing Couette flow as explained earlier. The τ_R for the same range of $\dot{\gamma}$ values (10^8 s^{-1} and 10^{11} s^{-1}) are found. The position vectors of the terminal carbon atoms are used for the computation of τ_R here as well.

Fig. 8 shows the values of τ_R as a function of $\dot{\gamma}$ at temperatures of 313 K and 373 K for polymer solution. The data is obtained as the average from three independent runs and the error bars show the standard deviation of the results from the three runs. The values at both the temperatures show huge error bars but a downward trend as a function of $\dot{\gamma}$. This implies that, as the shear forces on the polymer solution increase, the polymer tends to achieve an equilibrium configuration faster. Higher the relaxation time, stronger the elastic nature of the polymer chain. The changes in relaxation times as a function of both temperature and shear rate imply that the magnitude of vortices will vary with the operating conditions of the cooling liquids. Since the elastic instabilities facilitate the manifestation of vortical motion, the operating temperature and shear rates must be kept lower in magnitudes. Even though the relaxation time can be increased by polymer concentration, it can negatively influence the pumping losses.

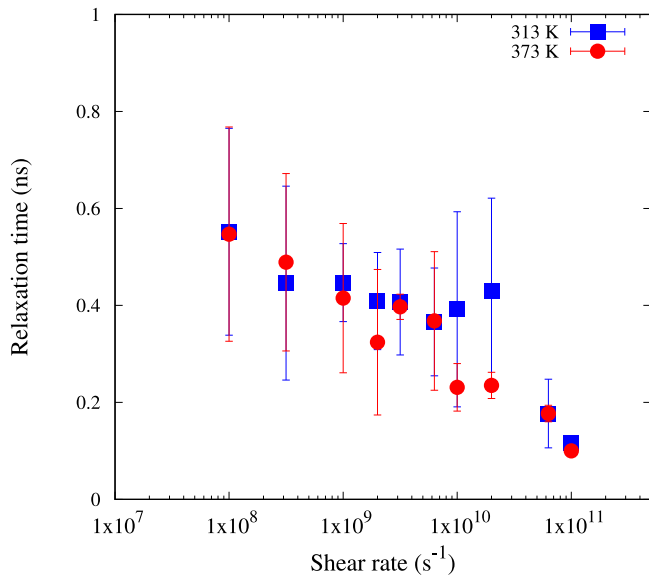


Fig. 8. The terminal relaxation time (τ_R) of OCP in the polymer solution as a function of shear rate at two different temperatures (313 K and 373 K).

3.7. Thermal conductivity

Having understood the rheological behaviour of the pure solvent and polymer solution systems, it is important to further know the thermal transfer properties. For a fluid oriented towards heat transfer applications, thermal conductivity (k) is a vital property to be computed. This metric provides a measure of the ability of a fluid to conduct heat given a temperature gradient across it. It is also necessary for the computation of the Nusselt number of novel liquids characterising the ratio of heat transfer via flow convection and conduction [93]. The conduction of heat is due to the microscopic behaviour of the material, making MD a useful tool to calculate it [94].

A methodology prescribed by Müller-Plathe [95] is considered as a reliable way to compute k in case of our systems. The formulation is based on the following relationship as given by Fourier's Law:

$$Q = k \frac{dT}{dx} \quad (20)$$

where, Q is the heat flux across the fluid and $\frac{dT}{dx} = \nabla T$ is the corresponding temperature gradient. Therefore, by implementing a temperature gradient which is linear across the simulation box, the consequent heat flux generated can be utilised to compute k . Müller-Plathe [95] proposed a way to implement the ∇T by routinely exchanging the translational velocities of the atoms in the simulation box. This ensures conservation of momentum as well. Over a long time period, the continuous exchange of the momentum leads to the development of a ∇T across the simulation box. This computational scheme is also referred as reverse-NEMD technique.

In our work, we consider the well-equilibrated and annealed systems from the equilibrium MD runs described in the section 'Simulation Details' as the initial configuration for the computation of k at the five different temperatures between 293 K and 373 K. For the sake of simplicity, we describe the procedure followed in case of the systems of pure PAO-2 solvent. The equilibrated and annealed pure solvent systems are further equilibrated for 1 ns under constant NVT conditions. The Nosé-Hoover thermostat is removed at this stage following which the heat flux as described by Müller-Plathe is implemented. The system is run for 2 ns under this condition where the centre of the box acts as the heat source and the box faces act as heat sinks. The entire box is divided into 20 layers along the z -direction and the momentum exchanges are applied at a frequency of every 200 time-steps across

Table 4

Mean values of $k_{polymer}$ of polymer solution at various temperatures.

Temperature (K)	$k_{polymer}$ ($W m^{-1} K^{-1}$)
293	-0.001
313	0.003
333	0.007
353	0.005
373	0.004

these layers (see Fig. 9). The temperature gradient is monitored at every 1000 time-steps. After 2 ns, the exchanges generate a linear ∇T , whereafter the production run is carried out for 10 ns. The reported values of k for a typical run are an average of the final 5 ns of the production run. The values converge well within an accuracy of $10^{-5} W m^{-1} K^{-1}$ after the first 2 ns of production runs. An identical procedure is followed in case of polymer solution system as well. The computed k as a function of temperature is shown in Fig. 9 for typical production runs for pure solvent at different temperatures.

Thermal conductivity of pure solvent decreases with temperature. This is in line with the behaviour of long-chain hydrocarbons in these conditions [96]. The drop in the thermal conductivity with increasing temperature is a consequence of the enhanced thermal motion of the atoms in the system [97]. This motion expands the liquid (signified by the decreasing density in Table 1) increasing the distance of immediate neighbours to transfer kinetic energy. The large error bars (standard deviation) in the computation are also observed in the experimental measurements of k of long chain hydrocarbons in liquid state as well [98]. The simulated data here is comparatively higher than the experimental data (0.137 – $0.132 W m^{-1} K^{-1}$) reported elsewhere [99]. The data can be fitted using a linear function

$$k = k_0 - \left(\frac{\partial k}{\partial T} \right)_p T \quad (21)$$

where, k_0 is the thermal conductivity at absolute zero and $\left(\frac{\partial k}{\partial T} \right)_p$ is the temperature coefficient at the atmospheric pressure, $p = 1$ atm. The temperature coefficient for the pure solvent system from the fit in Eq. (21) is $(1.8 \pm 0.03) \times 10^{-4} W m^{-1} K^{-2}$.

Fig. 9 also shows the variation of thermal conductivity in polymer solution as a function of temperature. The data shows that thermal conductivity of the solution is greater than that of the solvent at the various temperatures. The larger error bar at 293 K could be attributed to the insufficient time given for the system to evolve at very low temperatures and demands more sampling. Along with the enhancement in thermal conductivity at different temperatures compared to that of the solvent, fitting the data using Eq. (21) also shows a lower temperature coefficient, $\left(\frac{\partial k}{\partial T} \right)_p = (1.1 \pm 0.01) \times 10^{-4} W m^{-1} K^{-2}$ in case of the solution. This means that the reduction in thermal conductivity of the solution as a function of increasing temperature is slower in case of the polymer solution compared to that of the pure solvent.

Curtiss and Byron Bird [100] proposed the theory that in case of dilute polymer solutions, the thermal conductivity is an additive function. In other words,

$$k_{solution} = k_{solvent} + k_{polymer} \quad (22)$$

where $k_{solvent}$ and $k_{polymer}$ are the thermal conductivities of the solvent and polymer, respectively. This theory is predicted for Fraenkel and Hookean dumbbell model of chain polymers. From Eq. (22), we can obtain $k_{polymer}$ at different temperatures whose values are given in Table 4. Thermal conductivity enhancement in dilute polymer solutions is attributed to an increase in the contribution of the kinetic motion of the intra-molecular energy and the work done against the intra-molecular forces [101]. Also, $k_{polymer}$ is proportional to the chain stiffness. The contribution of $k_{polymer}$ Table 4 shows there are significant

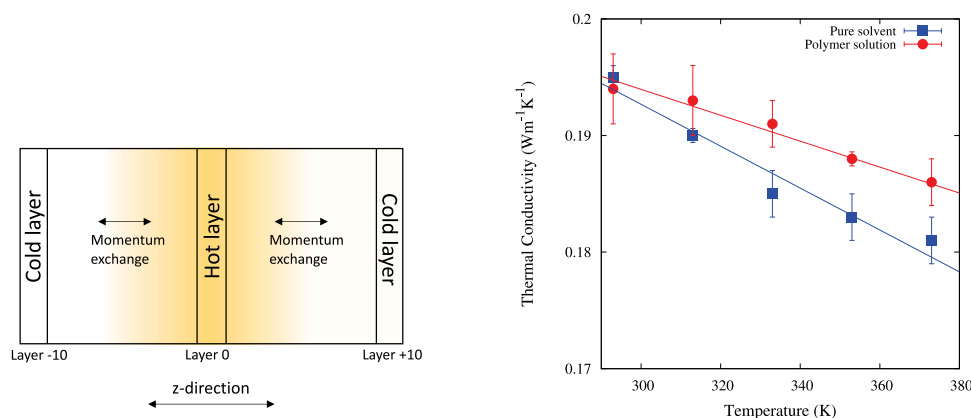


Fig. 9. (Left) The schematic of reverse-NEMD applied in case of the present simulation study. (Right) The thermal conductivity (k) of the pure solvent and polymer solution as a function of temperature. The closed symbols show the simulated data and the lines show the linear function fits as described in Eq. (21).

factors, in addition to chain stiffness helping in the thermal conductivity enhancement at different temperatures. Recent studies show the impact of monomer sequencing on the thermal conductivity of block polymers [102]. However, further studies are required to understand the effect of this in case of polymer solutions providing motivation for future works.

3.8. Advantages and limitations

The polymer addition leading to a weak non-Newtonian behaviour demonstrated in the past investigations of similar liquids [20] can have a measurable influence on vortex roll-up tendency in inertial flows. The MD study here is able to provide structural reasons for those observations that are difficult to be determined by experimental procedures. It establishes how the polymer addition to a synthetic oil changes the hydrodynamic radii of the solvent molecules. The impact of OCP as a thickening agent decreases with temperature as shown by the computation of Q_{VJ} . The shear thinning effect is enhanced by the addition of polymer chain that is correlated to the molecular alignment in the solution as a function of shear rates. The chain flexibility is prominent in case of OCP as determined by its hydrodynamic radius in the solution at all temperatures. Liquids having similar shear thinning indices (0.4–0.7), obtained by the comparison of m from the Carreau-model fit with Power law fit for a Herschel–Bulkley fluid, can provide Nusselt numbers between 40–60 for Reynolds number = 100 in case of immersion cooling which is better than what is observed for Newtonian fluids such as water [103]. At the same time, it is a limitation of the atomistic MD study to determine the actual composition of the polymer chain in the solution that may have optimal heat transfer properties. Moreover, computation of relaxation times of larger molecular weight polymer chains is also difficult in case of atomistic MD. This is where mesoscale modelling can help, and the models can be parametrised using the thermodynamic properties, viscosity and thermal conductivity obtained from atomistic MD, making this work significant.

4. Conclusion

The addition of an OCP polymer chain in PAO-2 solvent enhances the rheological properties of the resulting solution in the relevant temperature range. It improves the viscosity of polymer solution by increasing the hydrodynamic radii of the solvent molecules, effectively acting as a thickener to the base oil. Subsequently, the role of molecular stretching and alignment in the shear thinning behaviour of the liquids has been observed. The shear responses of the solvent and the polymer solution show that the latter starts shear thinning at a lower shear rate than the former. The better shear thinning nature of the dilute polymer solution emerging from their structural properties can contribute to

the evolution of coherent vortices, supporting their use in direct heat transfer applications. Simultaneously, the thermal conductivity of the solution is higher, and the decline in their values with rise in temperature is slower, compared to that of the base oil. This further justifies the use of mixtures made of OCP in PAO-2 as coolants. Even though the work signifies a viable direction in coolant research, the factors such as polymer composition needs to be determined based on the competing factors of thickening effect and shear thinning abilities. Such an analysis requires appropriate mesoscale studies that are part of our future works.

The analysis of the viscoelasticity of the polymer solution by the computation of the terminal relaxation time shows faster relaxation of the OCP chain with increasing temperature and shear rates. The storage and loss moduli of OCP polymer solution are higher than those of the pure solvent. The elastic nature of the OCP polymer increases the elastic instabilities of the polymer solution triggering coherent vortex formation. This in turn enhances the heat transfer process. Molecular dynamics guided design of dilute polymer mixtures that exhibit a clear viscoelastic nature can help in optimising the rheological behaviour of the liquid media suitable for effective thermal management in confined spaces related to immersion cooling.

CRedit authorship contribution statement

Bharath Ravikumar: Methodology, Validation, Data curation, Formal analysis, Investigation, Writing – original draft, Visualization. **Ioannis K. Karathanassis:** Conceptualization, Resources, Data curation, Writing – review & editing supervision, Project administration, Funding acquisition. **Timothy Smith:** Methodology, Investigation, Resources, Writing – review & editing. **Manolis Gavaises:** Supervision, Project administration, Funding acquisition, Writing – review & editing supervision.

Declaration of competing interest

The authors declare the following financial interests/personal relationships which may be considered as potential competing interests: Ioannis K. Karathanassis reports financial support was provided by EU Framework Programme for Research and Innovation HORIZON 2020. Timothy Smith reports a relationship with Lubrizol Ltd that includes: employment.

Data availability

Data will be made available on request.

Acknowledgements

The work has received funding from the EU Framework Programme for Research and Innovation HORIZON 2020 under the grant agreement No. 899659 (I-BAT project). The authors also acknowledge Flucon GmbH for conducting the experiments to compute thermodynamic properties.

Appendix A. Supplementary data

The Supporting Information document contains the L-OPLS-AA force field parameters, and the density of pure solvent systems at different pressures and modified Tait equation fits. The radial distribution functions of the carbon-carbon interactions of PAO-2 are present. The experimental determination of density and isothermal compressibility is also outlined. Furthermore, Arrhenius-model fits of kinematic viscosity, plots related to D_{COM} computations and the dynamic viscosity values obtained from different methods are presented. The end-to-end autocorrelation function and the corresponding sum of exponential fits of a simulation run are also plotted.

Supplementary material related to this article can be found online at <https://doi.org/10.1016/j.ijft.2023.100333>.

References

- [1] P. Birbarah, T. Gebrael, T. Foulkes, A. Stillwell, A. Moore, R. Pilawa-Podgurski, N. Miljkovic, Water immersion cooling of high power density electronics, *Int. J. Heat Mass Transfer* 147 (2020) 118918.
- [2] J.K. Mendizábal, M. Montazeri, D. Huitink, N. Miljkovic, Direct cooling of a planar magnetic converter using dielectric liquid forced convection enabled by additive manufacturing, *Int. J. Heat Mass Transfer* 191 (2022) 122809.
- [3] D. Shia, Y. Yang, S. Sivapalan, R. Soeung, C. Amoah-Kusi, Corrosion study on single-phase liquid cooling cold plates with inhibited propylene glycol/water coolant for data centers, *J. Manuf. Sci. Eng.* 143 (11) (2021).
- [4] Y. Deng, C. Feng, E. Jiaqiang, H. Zhu, J. Chen, M. Wen, H. Yin, Effects of different coolants and cooling strategies on the cooling performance of the power lithium ion battery system: A review, *Appl. Therm. Eng.* 142 (2018) 10–29.
- [5] D. Lee, Development of BLDC motor and multi-blade fan for HEV battery cooling system, *Int. J. Automot. Technol.* 15 (7) (2014) 1101–1106.
- [6] A. Manzoor, M. Saghir, Heat transfer enhancement in multiple pipes configuration using different fluid mixtures: A numerical approach, *Int. J. Thermofluids* 10 (2021) 100088.
- [7] W. Lin, B. Sunden, Vehicle cooling systems for reducing fuel consumption and carbon dioxide: literature survey, *SAE Tech. Pap.* (2010–01) (2010) 1509.
- [8] M. Lu, X. Zhang, J. Ji, X. Xu, Y. Zhang, Research progress on power battery cooling technology for electric vehicles, *J. Energy Storage* 27 (2020) 101155.
- [9] J. Smith, R. Singh, M. Hinterberger, M. Mochizuki, Battery thermal management system for electric vehicle using heat pipes, *Int. J. Therm. Sci.* 134 (2018) 517–529.
- [10] R. Van Gils, D. Danilov, P. Notten, M. Speetjens, H. Nijmeijer, Battery thermal management by boiling heat-transfer, *Energy Convers. Manage.* 79 (2014) 9–17.
- [11] C. Roe, X. Feng, G. White, R. Li, H. Wang, X. Rui, C. Li, F. Zhang, V. Null, M. Parkes, et al., Immersion cooling for lithium-ion batteries—A review, *J. Power Sources* 525 (2022) 231094.
- [12] X. Yin, C. Hu, M. Bai, J. Lv, An investigation on the heat transfer characteristics of nanofluids in flow boiling by molecular dynamics simulations, *Int. J. Heat Mass Transfer* 162 (2020) 120338.
- [13] K. Schmidmayer, P. Kumar, P. Lavielle, M. Miscevic, F. Topin, Heat transfer intensification in an actuated heat exchanger submitted to an imposed pressure drop, *PLoS One* 14 (7) (2019) e0219441.
- [14] S. Antoun, S. Srinivasan, M.Z. Saghir, A refined molecular dynamics approach to predict the thermophysical properties of positively charged alumina nanoparticles suspended in water, *Int. J. Thermofluids* 12 (2021) 100114.
- [15] R. Larson, *The Structure and Rheology of Complex Fluids*, in: *Topics in Chemical Engineering*, OUP USA, 1999, URL: <https://books.google.co.uk/books?id=BgTjwAEACAAJ>.
- [16] J. Niu, C. Fu, W. Tan, Slip-flow and heat transfer of a non-Newtonian nanofluid in a microtube, *PLoS One* 7 (5) (2012) e37274.
- [17] I. Mahbubul, R. Saidur, M. Amalina, Influence of particle concentration and temperature on thermal conductivity and viscosity of Al₂O₃/R141b nanorefrigerant, *Int. Commun. Heat Mass Transfer* 43 (2013) 100–104.
- [18] Z. Xu, K.S. Park, Y. Diao, What is the assembly pathway of a conjugated polymer from solution to thin films? *Front. Chem.* (2020) 1194.
- [19] H. Wu, C. Li, J. Li, Heat transfer enhancement by pulsating flow of a viscoelastic fluid in a microchannel with a rib plate, *Nanoscale Microscale Thermophys. Eng.* (2022) 1–17.
- [20] I. Karathanassis, E. Pashkovski, M. Heidari-Koochi, H. Jadidbonab, T. Smith, M. Gavaises, C. Bruecker, Non-Newtonian flow of highly-viscous oils in hydraulic components, *J. Non-Newton. Fluid Mech.* 275 (2020) 104221.
- [21] M.B. Khan, C. Sasmal, R. Chhabra, Flow and heat transfer characteristics of a rotating cylinder in a FENE-P type viscoelastic fluid, *J. Non-Newton. Fluid Mech.* 282 (2020) 104333.
- [22] H.A. Barnes, *A Handbook of Elementary Rheology*, Vol. 1, University of Wales, Institute of Non-Newtonian Fluid Mechanics Aberystwyth, 2000.
- [23] M. Hassan, F. Mebarek-Oudina, A. Faisal, A. Ghafar, A. Ismail, Thermal energy and mass transport of shear thinning fluid under effects of low to high shear rate viscosity, *Int. J. Thermofluids* 15 (2022) 100176.
- [24] T.A. Pimenta, J. Campos, Friction losses of Newtonian and non-Newtonian fluids flowing in laminar regime in a helical coil, *Exp. Therm Fluid Sci.* 36 (2012) 194–204.
- [25] Y.L. Xiong, C.-H. Bruneau, H. Kellay, A numerical study of two dimensional flows past a bluff body for dilute polymer solutions, *J. Non-Newton. Fluid Mech.* 196 (2013) 8–26.
- [26] M. Poreh, U. Paz, Turbulent heat transfer to dilute polymer solutions, *Int. J. Heat Mass Transfer* 11 (5) (1968) 805–818.
- [27] S. Parvar, C.B. da Silva, F. Pinho, Thermal boundary layer of laminar flow of dilute polymer solution, *Int. J. Heat Mass Transfer* 185 (2022) 122248.
- [28] F. Del Giudice, S.J. Haward, A.Q. Shen, Relaxation time of dilute polymer solutions: A microfluidic approach, *J. Rheol.* 61 (2) (2017) 327–337.
- [29] S. Antignard, G. Dupuis, C. Favéro, L. Rodríguez, B. Grassl, Portable rheometer to overcome the challenge of measuring low viscosity solution of acrylamide-based polymers at high temperature with an affordable cost for O&G applications, *J. Rheol.* 65 (5) (2021) 1053–1063.
- [30] S. Costanzo, G. Ianniruberto, G. Marrucci, D. Vlassopoulos, Measuring and assessing first and second normal stress differences of polymeric fluids with a modular cone-partitioned plate geometry, *Rheol. Acta* 57 (5) (2018) 363–376.
- [31] S.L. Anna, G.H. McKinley, Effect of a controlled pre-deformation history on extensional viscosity of dilute polymer solutions, *Rheol. Acta* 47 (8) (2008) 841–859.
- [32] R. Benda, J. Bullen, A. Plomer, Synthetics basics: Polyalphaolefins—base fluids for high-performance lubricants, *J. Synth. Lubr.* 13 (1) (1996) 41–57.
- [33] Y.S. Ko, W.-S. Kwon, M.-H. No, J.-H. Yim, A study on the control of microstructures of polyalphaolefins via cationic polymerization, *Polymer (Korea)* 39 (2) (2015) 346–352.
- [34] Synfluid PAO 2 cSt, No. MSDS # 100000010948, Chevron Phillips Chemical Company LP, 2019, URL: <https://www.cpchem.com/what-we-do/solutions/polyalphaolefins/products/synfluidr-pao-2-cst>.
- [35] M.J. Covitch, Olefin copolymer viscosity modifiers, in: *Lubricant Additives*, CRC Press, 2017, pp. 225–246, <http://dx.doi.org/10.1201/9781315120621-11>.
- [36] M. Negi, K.N. Kumar, A. Bhardwaj, G. Kapur, S. Ramakumar, Prediction of thickening efficiency of olefin copolymers and kinematic viscosities of the blended base oils by determining intrinsic viscosities of the copolymers in cyclohexane, *Egypt. J. Petrol.* 31 (2) (2022) 7–14.
- [37] M.J. Covitch, K.J. Trickett, et al., How polymers behave as viscosity index improvers in lubricating oils, *Adv. Chem. Eng. Sci.* 5 (02) (2015) 134.
- [38] A. Sen, I.D. Rubin, Molecular structures and solution viscosities of ethylene-propylene copolymers, *Macromolecules* 23 (9) (1990) 2519–2524.
- [39] U.S. Ramasamy, S. Lichter, A. Martini, Effect of molecular-scale features on the polymer coil size of model viscosity index improvers, *Tribol. Lett.* 62 (2) (2016) 1–7.
- [40] P. Panwar, P. Michael, M. Devlin, A. Martini, Critical shear rate of polymer-enhanced hydraulic fluids, *Lubricants* 8 (12) (2020) 102.
- [41] A.A. Pesaran, Battery thermal models for hybrid vehicle simulations, *J. Power Sources* 110 (2) (2002) 377–382.
- [42] Q. Wang, B. Jiang, B. Li, Y. Yan, A critical review of thermal management models and solutions of lithium-ion batteries for the development of pure electric vehicles, *Renew. Sustain. Energy Rev.* 64 (2016) 106–128.
- [43] S.C. Kim, Thermal performance of motor and inverter in an integrated starter generator system for a hybrid electric vehicle, *Energies* 6 (11) (2013) 6102–6119.
- [44] W.L. Jorgensen, D.S. Maxwell, J. Tirado-Rives, Development and testing of the OPLS all-atom force field on conformational energetics and properties of organic liquids, *J. Am. Chem. Soc.* 118 (45) (1996) 11225–11236.
- [45] S.W. Sit, K. Pluhackova, R.A. Böckmann, Optimization of the OPLS-AA force field for long hydrocarbons, *J. Chem. Theory Comput.* 8 (4) (2012) 1459–1470.
- [46] W.L. Jorgensen, J. Tirado-Rives, Molecular modeling of organic and biomolecular systems using BOSS and MCPRO, *J. Comput. Chem.* 26 (16) (2005) 1689–1700.
- [47] K. Pluhackova, H. Morhenn, L. Lautner, W. Lohstroh, K.S. Nemkovski, T. Unruh, R.A. Böckmann, Extension of the LOPLS-AA force field for alcohols, esters, and monoolein bilayers and its validation by neutron scattering experiments, *J. Phys. Chem. B* 119 (49) (2015) 15287–15299.

- [48] J.A. Rackers, Z. Wang, C. Lu, M.L. Laury, L. Lagardère, M.J. Schnieders, J.-P. Piquemal, P. Ren, J.W. Ponder, Tinker 8: software tools for molecular design, *J. Chem. Theory Comput.* 14 (10) (2018) 5273–5289.
- [49] S.S. Scheuermann, S. Eibl, P. Bartl, Detailed characterisation of isomers present in polyalphaolefin dimer and the effect of isomeric distribution on bulk properties, *Lubr. Sci.* 23 (5) (2011) 221–232.
- [50] D. Mathas, W. Holweger, M. Wolf, C. Bohnert, V. Bakolas, J. Procelewska, L. Wang, S. Bair, C.-K. Skylaris, Evaluation of methods for viscosity simulations of lubricants at different temperatures and pressures: a case study on PAO-2, *Tribol. Trans.* 64 (6) (2021) 1138–1148.
- [51] A.I. Jewett, D. Stelter, J. Lambert, S.M. Saladi, O.M. Roscioni, M. Ricci, L. Autin, M. Maritan, S.M. Bashusqeh, T. Keyes, et al., Moltemplate: A tool for coarse-grained modeling of complex biological matter and soft condensed matter physics, *J. Mol. Biol.* 433 (11) (2021) 166841.
- [52] S. Plimpton, Fast parallel algorithms for short-range molecular dynamics, *J. Comput. Phys.* 117 (1) (1995) 1–19.
- [53] B.A. Luty, W.F. van Gunsteren, Calculating electrostatic interactions using the particle-particle-particle-mesh method with nonperiodic long-range interactions, *J. Phys. Chem.* 100 (7) (1996) 2581–2587.
- [54] L. Verlet, Computer experiments on classical fluids. I. Thermodynamical properties of Lennard-Jones molecules, *Phys. Rev.* 159 (1) (1967) 98.
- [55] M. Len, U.S. Ramasamy, S. Lichter, A. Martini, Thickening mechanisms of polyisobutylene in polyalphaolefin, *Tribol. Lett.* 66 (1) (2018) 1–9.
- [56] L. Mohammed, H. Nourddine, D. Abdelali, R. Hamid, et al., Chitosan-covered liposomes as a promising drug transporter: Nanoscale investigations, *RSC Adv.* 11 (3) (2021) 1503–1516.
- [57] S.S. Bair, *High Pressure Rheology for Quantitative Elastohydrodynamics*, Elsevier, 2019.
- [58] J. Dymond, R. Malhotra, The tait equation: 100 years on, *Int. J. Thermophys.* 9 (6) (1988) 941–951.
- [59] A. Bakak, M. Lotfi, R. Heyd, A. Ammar, A. Koumina, Viscosity and rheological properties of graphene nanopowders nanofluids, *Entropy* 23 (8) (2021) 979.
- [60] S. Hamze, D. Cabaleiro, P. Estellé, Graphene-based nanofluids: A comprehensive review about rheological behavior and dynamic viscosity, *J. Mol. Liq.* 325 (2021) 115207.
- [61] S. Temkin, S. Temkin, *Elements of Acoustics*, Wiley New York, 1981.
- [62] J.-P. Rivet, Green-Kubo formalism for lattice gas hydrodynamics and Monte-Carlo evaluation of shear viscosities, *Complex Syst.* 1 (1987) 839–851.
- [63] Y. Nakamura, S. Hiraiwa, F. Suzuki, M. Matsui, High-pressure viscosity measurements of polyalphaolefins at elevated temperature, *Tribol. Online* 11 (2) (2016) 444–449.
- [64] P. Luo, Y. Gu, Effects of asphaltene content on the heavy oil viscosity at different temperatures, *Fuel* 86 (7–8) (2007) 1069–1078.
- [65] I.O. Igwe, The effects of temperature on the viscosity of vegetable oils in solution, *Ind. Crop. Prod.* 19 (2) (2004) 185–190.
- [66] T. Budtova, P. Navard, Viscosity-temperature dependence and activation energy of cellulose solutions, *Nord. Pulp Pap. Res. J.* 30 (1) (2015) 99–104.
- [67] A. Tager, V.Y. Dreval, F. Khasina, Concentrated polymer solutions—III. Viscosity of polyisobutylene solutions in various solvents, *Polym. Sci. USSR* 4 (5) (1963) 1097–1106.
- [68] D. Frenkel, B. Smit, *Understanding Molecular Simulation: From Algorithms To Applications*, Vol. 1, Elsevier, 2001.
- [69] B. Ravikumar, M. Mynam, S. Repaka, B. Rai, Solvation shell dynamics explains charge transport characteristics of LIB electrolytes, *J. Mol. Liq.* 338 (2021) 116613.
- [70] A. Lees, S. Edwards, The computer study of transport processes under extreme conditions, *J. Phys. C: Solid State Phys.* 5 (15) (1972) 1921.
- [71] A.J. Wagner, I. Pagonabarraga, Lees-Edwards boundary conditions for lattice Boltzmann, *J. Stat. Phys.* 107 (1) (2002) 521–537.
- [72] P.J. Davis, B. Todd, A simple, direct derivation and proof of the validity of the SLLOD equations of motion for generalized homogeneous flows, *J. Chem. Phys.* 124 (19) (2006) 194103.
- [73] D.J. Evans, G. Morriss, Nonlinear-response theory for steady planar couette flow, *Phys. Rev. A* 30 (3) (1984) 1528.
- [74] P. Santak, G. Conduit, Enhancing NEMD with automatic shear rate sampling to model viscosity and correction of systematic errors in modeling density: Application to linear and light branched alkanes, *J. Chem. Phys.* 153 (1) (2020) 014102.
- [75] B. Purnode, M. Crochet, Polymer solution characterization with the FENE-P model, *J. Non-Newton. Fluid Mech.* 77 (1–2) (1998) 1–20.
- [76] S. Sen, S.K. Kumar, P. Koblinski, Viscoelastic properties of polymer melts from equilibrium molecular dynamics simulations, *Macromolecules* 38 (3) (2005) 650–653.
- [77] P. Liu, J. Lu, H. Yu, N. Ren, F.E. Lockwood, Q.J. Wang, Lubricant shear thinning behavior correlated with variation of radius of gyration via molecular dynamics simulations, *J. Chem. Phys.* 147 (8) (2017) 084904.
- [78] S. Cui, S. Gupta, P. Cummings, H. Cochran, Molecular dynamics simulations of the rheology of normal decane, hexadecane, and tetracosane, *J. Chem. Phys.* 105 (3) (1996) 1214–1220.
- [79] J. Moore, S. Cui, H. Cochran, P. Cummings, Rheology of lubricant basestocks: A molecular dynamics study of C 30 isomers, *J. Chem. Phys.* 113 (19) (2000) 8833–8840.
- [80] N. Marx, L. Fernández, F. Barceló, H. Spikes, Shear thinning and hydrodynamic friction of viscosity modifier-containing oils. Part I: shear thinning behaviour, *Tribol. Lett.* 66 (3) (2018) 1–14.
- [81] T. Selby, The non-Newtonian characteristics of lubricating oils, *ASLE Trans.* 1 (1) (1958) 68–81.
- [82] P.J. Flory, *Principles of Polymer Chemistry*, Cornell University Press, 1953.
- [83] S. Rizvi, A Comprehensive Review of Lubricant Chemistry, Technology, Selection, and Design, in: *ASTM Manual Series*, ASTM International, 2009, URL: <https://books.google.co.in/books?id=KKLjvQEACAAJ>.
- [84] J. Dale, The conformational consequences of replacing methylene groups by ether oxygen, *Tetrahedron* 30 (12) (1974) 1683–1694.
- [85] C.-C. Huang, G. Gompper, R.G. Winkler, Non-equilibrium relaxation and tumbling times of polymers in semidilute solution, *J. Phys.: Condens. Matter* 24 (28) (2012) 284131.
- [86] X. Kong, Y. Han, W. Chen, F. Cui, Y. Li, Understanding conformational and dynamical evolution of semiflexible polymers in shear flow, *Soft Matter* 15 (31) (2019) 6353–6361.
- [87] R.G. Winkler, D.A. Fedosov, G. Gompper, Dynamical and rheological properties of soft colloid suspensions, *Curr. Opin. Colloid Interface Sci.* 19 (6) (2014) 594–610.
- [88] R. Datta, L. Yelash, F. Schmid, F. Kummer, M. Oberlack, M. Lukáčová-Medvid'ová, P. Virnau, Shear-thinning in oligomer melts—Molecular origins and applications, *Polymers* 13 (16) (2021) 2806.
- [89] J. Snoeijer, A. Pandey, M. Herrada, J. Eggers, The relationship between viscoelasticity and elasticity, *Proc. R. Soc. Lond. Ser. A Math. Phys. Eng. Sci.* 476 (2243) (2020) 20200419.
- [90] A. Mordvinkin, D. Döhler, W.H. Binder, R.H. Colby, K. Saalwächter, Terminal flow of cluster-forming supramolecular polymer networks: Single-chain relaxation or micelle reorganization? *Phys. Rev. Lett.* 125 (12) (2020) 127801.
- [91] J. Zilz, C. Schäfer, C. Wagner, R.J. Poole, M.A. Alves, A. Lindner, Serpentine channels: micro-rheometers for fluid relaxation times, *Lab Chip* 14 (2) (2014) 351–358.
- [92] F. Del Giudice, G. D'Avino, F. Greco, I. De Santo, P.A. Netti, P.L. Maffettone, Rheometry-on-a-chip: measuring the relaxation time of a viscoelastic liquid through particle migration in microchannel flows, *Lab Chip* 15 (3) (2015) 783–792.
- [93] L. Pekar, *Advanced Analytic and Control Techniques for Thermal Systems with Heat Exchangers*, Academic Press, 2020.
- [94] T.S. Komatsu, N. Nakagawa, S.-i. Sasa, H. Tasaki, Steady-state thermodynamics for heat conduction: microscopic derivation, *Phys. Rev. Lett.* 100 (23) (2008) 230602.
- [95] F. Müller-Plathe, A simple nonequilibrium molecular dynamics method for calculating the thermal conductivity, *J. Chem. Phys.* 106 (14) (1997) 6082–6085.
- [96] Y. Wada, Y. Nagasaka, A. Nagashima, Measurements and correlation of the thermal conductivity of liquid n-paraffin hydrocarbons and their binary and ternary mixtures, *Int. J. Thermophys.* 6 (3) (1985) 251–265.
- [97] M.R. Rao, Thermal conductivity of liquids, *J. Chem. Phys.* 9 (1) (1941) 120–121.
- [98] C. Vélez, M. Khayet, J.O. De Zárate, Temperature-dependent thermal properties of solid/liquid phase change even-numbered n-alkanes: n-hexadecane, n-octadecane and n-eicosane, *Appl. Energy* 143 (2015) 383–394.
- [99] E. Booser, *Tribology Data Handbook: An Excellent Friction, Lubrication, and Wear Resource*, CRC Press, 1997, URL: <https://books.google.co.uk/books?id=VRmLriy00pQC>.
- [100] C.F. Curtiss, R. Byron Bird, Thermal conductivity of dilute solutions of chainlike polymers, *J. Chem. Phys.* 107 (13) (1997) 5254–5267.
- [101] R. Byron, B.C.F. Curtiss, K.J. Beers, Polymer contribution to the thermal conductivity and viscosity in a dilute solution (Fraenkel Dumbbell model), *Rheol. Acta* 36 (3) (1997) 269–276.
- [102] T. Zhou, Z. Wu, H.K. Chilukoti, F. Müller-Plathe, Sequence-engineering polyethylene-polypropylene copolymers with high thermal conductivity using a molecular-dynamics-based genetic algorithm, *J. Chem. Theory Comput.* 17 (6) (2021) 3772–3782.
- [103] N. Nirmalkar, R. Chhabra, R. Poole, Effect of shear-thinning behaviour on heat transfer from a heated sphere in a yield-stress fluids, *Ind. Eng. Chem. Res.* 52 (37) (2013) 13490–13504.